

RADAR IMAGING VIA ADAPTIVE MIMO TECHNIQUES

Luzhou Xu, Jian Li

Dept. of Electrical and Computer Engineering,
P. O. Box 116130, University of Florida,
Gainesville, FL 32611, USA.

Petre Stoica

Dept. of Information Technology,
Uppsala University, P. O. Box 337,
SE-75105, Uppsala, Sweden.

ABSTRACT

We investigate several adaptive techniques for a multiple-input multiple-output (MIMO) radar system. By transmitting independent waveforms via different antennas, the echoes due to targets at different locations are linearly independent of each other, which allows the direct application of many adaptive techniques. We discuss several adaptive radar imaging algorithms, which can provide excellent estimation accuracy of both target locations and target amplitudes, and high robustness to the array calibration errors. To reject the false peaks due to the strong jammers, we also propose a generalized likelihood ratio test (GLRT). As shown by the numerical examples, the number of targets can be estimated accurately by using GLRT, and an accurate description of the target scenario can be obtained by combining the adaptive radar imaging algorithms and the GLRT technique.

1. INTRODUCTION

A multiple-input and multiple-output (MIMO) radar uses multiple antennas to simultaneously transmit several (possibly linearly independent) waveforms and it also uses multiple antennas to receive the reflected signals (see, e.g., [1] [2] [3] and the references therein). Many MIMO schemes have been proposed to resist the target's scintillations [1], to generate a desired transmitting beam-pattern [2], or to achieve a high-resolution spatial spectrum estimation [3].

We consider herein a new MIMO radar scheme that can deal with multiple targets. Similar to some of the aforementioned MIMO radar approaches, linearly independent waveforms are transmitted simultaneously via multiple antennas. Due to the different phase shifts associated with the different propagation paths from the transmitting antennas to targets, these independent waveforms are linearly combined at the targets with different phase factors. As a result, the signal waveforms reflected from different targets are linearly independent of each other, which allows for the application of Capon and of other adaptive array algorithms. We consider applying two well-known adaptive approaches,

i.e., the Capon and APES (Amplitude and Phase Estimation) [4] algorithms, to the proposed MIMO radar system to estimate the target locations and the reflected signal amplitudes. Then a generalized likelihood ratio test (GLRT) is derived, which, as shown via numerical examples, can be used to determine the number of targets by separating jammers from targets.

We also investigate robust adaptive methods in the presence of array calibration errors. It is well-known that the performance of Capon degrades severely in the presence of steering vector errors. This problem also affects APES and other adaptive methods, but to a lesser extent. In the presence of array calibration errors, we suggest the use of the recently proposed robust Capon beamformer (RCB) (see [5], [6] and references therein) to process the MIMO radar data. As shown in the numerical examples, when array calibration errors are present, RCB significantly outperforms the aforementioned (non-robust) adaptive methods.

The remainder of this paper is organized as follows. In Section 2, we describe our MIMO radar scheme and the associated data model. Several adaptive methods and a robust adaptive methods are presented in Sections 3 and 4, respectively. We provide several numerical examples in Section 5. Finally, Section 6 contains our conclusions.

2. SIGNAL MODEL

Consider a MIMO narrowband radar system with N arbitrarily located transmitting antennas and M arbitrarily located receiving antennas. The system simultaneously transmits N linearly independent waveforms, denoted by $\mathbf{s}_n \in \mathcal{C}^{L \times 1}$ ($n = 1, 2, \dots, N$) with L being the snapshot number. Let θ be the location parameter of a generic target, for example, the direction of arrival (DOA) when the targets are in the far field of the arrays, and let $\mathbf{a}_t(\theta)$ be the corresponding steering vector for the transmitting antenna array. Then the waveform vector of the reflected signals from the target at θ is $\mathbf{a}_t^T(\theta)\mathbf{S}$ with $(\cdot)^T$ denoting the transpose and $\mathbf{S} = [\mathbf{s}_1 \ \mathbf{s}_2 \ \dots \ \mathbf{s}_N]^T$. Note that $\mathbf{a}_t^T(\theta)\mathbf{S}$ is a function of the location parameter θ . Hence, the signals reflected from tar-

Please address all correspondences to Dr. Jian Li.

gets at different locations are linearly independent of each other. By assuming that the targets are located in the same range bin, the reflected signals arrive at the receiving array at about the same time and the arrival time is known.

The signal matrix at the output of the receiving array has the form:

$$\mathbf{X} = \mathbf{a}_r(\theta)\beta(\theta)\mathbf{a}_t^T(\theta)\mathbf{S} + \mathbf{Z}, \quad (1)$$

where the columns of $\mathbf{X} \in \mathcal{C}^{M \times L}$ are the received data snapshots, $\mathbf{a}_r(\theta) \in \mathcal{C}^{M \times 1}$ is the steering vector of the receiving antenna array and $\beta(\theta) \in \mathcal{C}$ denotes the complex amplitude of the reflected signal from θ , i.e., the ‘‘reflection coefficient’’ of the focal point θ . The matrix $\mathbf{Z} \in \mathcal{C}^{M \times L}$ denotes the residual term, which includes the unmodelled noise, interferences from targets at locations other than θ , and intentional or unintentional jamming. For notional simplicity, we will not show explicitly the dependence of \mathbf{Z} on θ .

The problem is to estimate $\beta(\theta)$ for each θ of interest from the observed data matrix \mathbf{X} . The estimates of $\{\beta(\theta)\}$ can be used to form a spatial spectrum in the 1D case or a radar image in the 2D case. We can then estimate the locations of the targets and their ‘‘reflection coefficients’’ by searching for the peaks in the so-obtained spectrum (or image).

We remark that we can first apply matched-filters to (1). Then the data model in (1) becomes:

$$\mathbf{Y} \triangleq \frac{1}{L}\mathbf{X}\mathbf{S}^H = \mathbf{a}_r(\theta)\beta(\theta)\mathbf{a}_t^T(\theta)\mathbf{R}_{SS} + \mathbf{Z}\mathbf{S}^H, \quad (2)$$

where $\mathbf{R}_{SS} = \frac{1}{L}\mathbf{S}\mathbf{S}^H$ is the covariance matrix of the transmitted waveforms. Note that (2) has the same form as (1). Hence, the methods introduced below can also be applied to \mathbf{Y} .

3. ADAPTIVE APPROACHES IN THE ABSENCE OF ARRAY CALIBRATION ERRORS

We assume below that the steering vectors are known precisely, and present adaptive methods.

3.1. Capon

The Capon beamformer can be formulated as follows:

$$\min_{\mathbf{w}} \mathbf{w}^H \hat{\mathbf{R}} \mathbf{w} \quad \text{subject to} \quad \mathbf{w}^H \mathbf{a}_r(\theta) = 1, \quad (3)$$

where $(\cdot)^H$ denotes the conjugate transpose and $\mathbf{w} \in \mathcal{C}^{M \times 1}$ is the weight vector used to achieve noise, interference and jamming suppression while keeping the desired signal undistorted, and $\hat{\mathbf{R}}$ is the sample covariance of the observed snapshots, i.e., $\hat{\mathbf{R}} = \frac{1}{L}\mathbf{X}\mathbf{X}^H$.

Solving (3), we can readily obtain the solution to (3) as follows:

$$\hat{\mathbf{w}}_{\text{capon}} = \frac{\hat{\mathbf{R}}^{-1}\mathbf{a}_r(\theta)}{\mathbf{a}_r^H(\theta)\hat{\mathbf{R}}^{-1}\mathbf{a}_r(\theta)}. \quad (4)$$

Applying the LS method to the signal at the output of the beamformer, i.e., $\hat{\mathbf{w}}_{\text{capon}}^H \mathbf{X}$ yields the Capon estimate of $\beta(\theta)$:

$$\hat{\beta}_{\text{capon}}(\theta) = \frac{\mathbf{a}_r^H(\theta)\hat{\mathbf{R}}^{-1}\mathbf{X}\mathbf{S}^H\mathbf{a}_t^*(\theta)}{L[\mathbf{a}_r^H(\theta)\hat{\mathbf{R}}^{-1}\mathbf{a}_r(\theta)][\mathbf{a}_t^T(\theta)\hat{\mathbf{R}}_{SS}\mathbf{a}_t^*(\theta)]}, \quad (5)$$

where $(\cdot)^*$ denotes the complex conjugate.

3.2. APES

By following [7], the APES method can be formulated as:

$$\min_{\mathbf{w}, \beta} \|\mathbf{w}^H \mathbf{X} - \beta(\theta)\mathbf{a}_t^T(\theta)\mathbf{S}\|^2 \quad \text{subject to} \quad \mathbf{w}^H \mathbf{a}_r(\theta) = 1, \quad (6)$$

where $\mathbf{w} \in \mathcal{C}^{M \times 1}$ is the weight vector. Intuitively, the goal of (6) is to find a beamformer whose output is as close as possible to a signal with the waveform given by $\mathbf{a}_t^T(\theta)\mathbf{S}$.

Solving the optimization problem in (6) yields the APES estimate of β as follows:

$$\hat{\beta}_{\text{APES}}(\theta) = \frac{\mathbf{a}_r^H(\theta)\hat{\mathbf{Q}}^{-1}\mathbf{X}\mathbf{S}^H\mathbf{a}_t^*(\theta)}{L[\mathbf{a}_r^H(\theta)\hat{\mathbf{Q}}^{-1}\mathbf{a}_r(\theta)][\mathbf{a}_t^T(\theta)\hat{\mathbf{R}}_{SS}\mathbf{a}_t^*(\theta)]}, \quad (7)$$

where

$$\hat{\mathbf{Q}} = \hat{\mathbf{R}} - \frac{\mathbf{X}\mathbf{S}^H\mathbf{a}_t^*(\theta)\mathbf{a}_t^T(\theta)\mathbf{S}\mathbf{X}^H}{L^2\mathbf{a}_t^T(\theta)\hat{\mathbf{R}}_{SS}\mathbf{a}_t^*(\theta)}. \quad (8)$$

3.3. Generalized Likelihood Ratio Test

In this subsection, we assume that the columns of the residual term \mathbf{Z} in (1) are independently and identically distributed circularly symmetric complex Gaussian random vectors with zero-mean and unknown covariance matrix \mathbf{Q} . We derive the GLRT for each θ of interest. For notational brevity, we omit the argument θ of ρ , \mathbf{a}_r , \mathbf{a}_t and β in this subsection.

Following [8] (see also [9]), we define the GLR as follows:

$$\rho = 1 - \left[\frac{\max_{\mathbf{Q}} f(\mathbf{X}|\beta = 0, \mathbf{Q})}{\max_{\beta, \mathbf{Q}} f(\mathbf{X}|\beta, \mathbf{Q})} \right]^{\frac{1}{L}}, \quad (9)$$

where

$$f(\mathbf{X}|\beta, \mathbf{Q}) = \pi^{-LM} |\mathbf{Q}|^{-L} \exp \left\{ -\text{tr} \left[\mathbf{Q}^{-1} (\mathbf{X} - \mathbf{a}_r\beta\mathbf{a}_t^T\mathbf{S})(\mathbf{X} - \mathbf{a}_r\beta\mathbf{a}_t^T\mathbf{S})^H \right] \right\} \quad (10)$$

is the probability density function of the observed data matrix \mathbf{X} given the parameters β and \mathbf{Q} , and $\text{tr}(\cdot)$ and $|\cdot|$ denote the trace and determinant of a matrix, respectively. From (9), we note that the value of the GLR, ρ , lies between 0 and 1. If there is a target at a θ of interest, we usually have

$\max_{\beta, \mathbf{Q}} f(\mathbf{X}|\beta, \mathbf{Q}) \gg \max_{\mathbf{Q}} f(\mathbf{X}|\beta = 0, \mathbf{Q})$, i.e., $\rho \approx 1$; otherwise $\rho \approx 0$.

Solving the optimization problems in (9) with respect to \mathbf{Q} yields

$$\max_{\mathbf{Q}} f(\mathbf{X}|\beta = 0, \mathbf{Q}) = (\pi e)^{-LM} |\hat{\mathbf{R}}|^{-L}, \quad (11)$$

and

$$\begin{aligned} \max_{\beta, \mathbf{Q}} f(\mathbf{X}|\beta, \mathbf{Q}) &= (\pi e)^{-LM} \\ &\left\{ \min_{\beta} \left| \frac{1}{L} (\mathbf{X} - \mathbf{a}_r \beta \mathbf{a}_t^T \mathbf{S}) (\mathbf{X} - \mathbf{a}_r \beta \mathbf{a}_t^T \mathbf{S})^H \right| \right\}^{-L}. \end{aligned} \quad (12)$$

Note that

$$\begin{aligned} &\left| \frac{1}{L} (\mathbf{X} - \mathbf{a}_r \beta \mathbf{a}_t^T \mathbf{S}) (\mathbf{X} - \mathbf{a}_r \beta \mathbf{a}_t^T \mathbf{S})^H \right| \\ &= |\hat{\mathbf{Q}} + (\mathbf{a}_t^T \hat{\mathbf{R}}_{SS} \mathbf{a}_t^*)| \\ &\quad \left(\mathbf{a}_r \beta - \frac{\mathbf{X} \mathbf{S}^H \mathbf{a}_t^*}{L(\mathbf{a}_t^T \hat{\mathbf{R}}_{SS} \mathbf{a}_t^*)} \right) \left(\mathbf{a}_r \beta - \frac{\mathbf{X} \mathbf{S}^H \mathbf{a}_t^*}{L(\mathbf{a}_t^T \hat{\mathbf{R}}_{SS} \mathbf{a}_t^*)} \right)^H \\ &= |\hat{\mathbf{Q}}| \left| \mathbf{I} + (\mathbf{a}_t^T \hat{\mathbf{R}}_{SS} \mathbf{a}_t^*) \hat{\mathbf{Q}}^{-1} \right. \\ &\quad \left. \left(\mathbf{a}_r \beta - \frac{\mathbf{X} \mathbf{S}^H \mathbf{a}_t^*}{L(\mathbf{a}_t^T \hat{\mathbf{R}}_{SS} \mathbf{a}_t^*)} \right) \left(\mathbf{a}_r \beta - \frac{\mathbf{X} \mathbf{S}^H \mathbf{a}_t^*}{L(\mathbf{a}_t^T \hat{\mathbf{R}}_{SS} \mathbf{a}_t^*)} \right)^H \right| \\ &= |\hat{\mathbf{Q}}| \left[1 + (\mathbf{a}_t^T \hat{\mathbf{R}}_{SS} \mathbf{a}_t^*) \right. \\ &\quad \left. \left(\mathbf{a}_r \beta - \frac{\mathbf{X} \mathbf{S}^H \mathbf{a}_t^*}{L(\mathbf{a}_t^T \hat{\mathbf{R}}_{SS} \mathbf{a}_t^*)} \right)^H \hat{\mathbf{Q}}^{-1} \left(\mathbf{a}_r \beta - \frac{\mathbf{X} \mathbf{S}^H \mathbf{a}_t^*}{L(\mathbf{a}_t^T \hat{\mathbf{R}}_{SS} \mathbf{a}_t^*)} \right) \right] \\ &\geq |\hat{\mathbf{Q}}| \left[1 + \frac{\mathbf{a}_t^T \mathbf{S} \mathbf{X}^H}{L^2(\mathbf{a}_t^T \hat{\mathbf{R}}_{SS} \mathbf{a}_t^*)} \hat{\mathbf{Q}}^{-1} \left(\mathbf{I} - \frac{\mathbf{a}_r \mathbf{a}_r^H \hat{\mathbf{Q}}^{-1}}{\mathbf{a}_r^H \hat{\mathbf{Q}}^{-1} \mathbf{a}_r} \right) \mathbf{X} \mathbf{S}^H \mathbf{a}_t^* \right], \end{aligned} \quad (13)$$

where we have used the fact that $|\mathbf{I} + \mathbf{A}\mathbf{B}| = |\mathbf{I} + \mathbf{B}\mathbf{A}|$, and the equality holds when $\beta = \hat{\beta}_{\text{APES}}$. Note that the right side of the inequality in (13) can be simplified as follows:

$$\begin{aligned} (13) &= |\hat{\mathbf{Q}}| \left[1 + \frac{\mathbf{a}_t^T \mathbf{S} \mathbf{X}^H}{L^2(\mathbf{a}_t^T \hat{\mathbf{R}}_{SS} \mathbf{a}_t^*)} \right. \\ &\quad \left. \hat{\mathbf{Q}}^{-1} \left(\mathbf{I} - \frac{\mathbf{a}_r \mathbf{a}_r^H \hat{\mathbf{Q}}^{-1}}{\mathbf{a}_r^H \hat{\mathbf{Q}}^{-1} \mathbf{a}_r} \right) \mathbf{X} \mathbf{S}^H \mathbf{a}_t^* \right] \\ &= \left| \hat{\mathbf{Q}} + \left(\mathbf{I} - \frac{\mathbf{a}_r \mathbf{a}_r^H \hat{\mathbf{Q}}^{-1}}{\mathbf{a}_r^H \hat{\mathbf{Q}}^{-1} \mathbf{a}_r} \right) \frac{\mathbf{X} \mathbf{S}^H \mathbf{a}_t^* \mathbf{a}_t^T \mathbf{S} \mathbf{X}^H}{L^2(\mathbf{a}_t^T \hat{\mathbf{R}}_{SS} \mathbf{a}_t^*)} \right| \\ &= \left| \hat{\mathbf{R}} - \frac{\mathbf{a}_r \mathbf{a}_r^H \hat{\mathbf{Q}}^{-1} \mathbf{X} \mathbf{S}^H \mathbf{a}_t^* \mathbf{a}_t^T \mathbf{S} \mathbf{X}^H}{L^2(\mathbf{a}_r^H \hat{\mathbf{Q}}^{-1} \mathbf{a}_r) (\mathbf{a}_t^T \hat{\mathbf{R}}_{SS} \mathbf{a}_t^*)} \right| \\ &= |\hat{\mathbf{R}}| \left| \mathbf{I} - \frac{\hat{\mathbf{R}}^{-1} \mathbf{a}_r \mathbf{a}_r^H \hat{\mathbf{Q}}^{-1} \mathbf{X} \mathbf{S}^H \mathbf{a}_t^* \mathbf{a}_t^T \mathbf{S} \mathbf{X}^H}{L^2(\mathbf{a}_r^H \hat{\mathbf{Q}}^{-1} \mathbf{a}_r) (\mathbf{a}_t^T \hat{\mathbf{R}}_{SS} \mathbf{a}_t^*)} \right| \\ &= |\hat{\mathbf{R}}| \left[1 - \frac{\mathbf{a}_r^H \hat{\mathbf{Q}}^{-1} (\hat{\mathbf{R}} - \hat{\mathbf{Q}}) \hat{\mathbf{R}}^{-1} \mathbf{a}_r}{\mathbf{a}_r^H \hat{\mathbf{Q}}^{-1} \mathbf{a}_r} \right] \\ &= |\hat{\mathbf{R}}| \frac{\mathbf{a}_r^H \hat{\mathbf{R}}^{-1} \mathbf{a}_r}{\mathbf{a}_r^H \hat{\mathbf{Q}}^{-1} \mathbf{a}_r} \end{aligned} \quad (14)$$

where we have used (8) and the fact that $|\mathbf{I} + \mathbf{A}\mathbf{B}| = |\mathbf{I} + \mathbf{B}\mathbf{A}|$.

From (13) and (14), it follows that

$$\begin{aligned} &\min_{\beta} \left| \frac{1}{L} (\mathbf{X} - \mathbf{a}_r \beta \mathbf{a}_t^T \mathbf{S}) (\mathbf{X} - \mathbf{a}_r \beta \mathbf{a}_t^T \mathbf{S})^H \right| \\ &= |\hat{\mathbf{R}}| \frac{\mathbf{a}_r^H \hat{\mathbf{R}}^{-1} \mathbf{a}_r}{\mathbf{a}_r^H \hat{\mathbf{Q}}^{-1} \mathbf{a}_r}. \end{aligned} \quad (15)$$

By using (11), (12), and (15) in (9), the GLR in (16) follows:

$$\rho(\theta) = 1 - \frac{\mathbf{a}_r^H(\theta) \hat{\mathbf{R}}^{-1} \mathbf{a}_r(\theta)}{\mathbf{a}_r^H(\theta) \hat{\mathbf{Q}}^{-1} \mathbf{a}_r(\theta)}. \quad (16)$$

4. ADAPTIVE APPROACHES IN THE PRESENCE OF ARRAY CALIBRATION ERRORS

The previous adaptive methods assume that the transmitting and receiving arrays are perfectly calibrated, i.e., $\mathbf{a}_t(\theta)$ and $\mathbf{a}_r(\theta)$ are accurately known as functions of θ . However, in practice, array calibration errors are often inevitable. The presence of array calibration errors and the related small snapshot number problem can degrade significantly the performance of the adaptive methods discussed so far.

We consider the application of the robust Capon beamformer (RCB) (see [5], [6] and references therein) to a MIMO radar system that suffers from calibration errors. RCB allows $\mathbf{a}_r(\theta)$ to lie in an uncertainty set. Without loss of generality, we assume that $\mathbf{a}_r(\theta)$ belongs to an uncertainty sphere:

$$\| \mathbf{a}_r(\theta) - \bar{\mathbf{a}}_r(\theta) \|^2 \leq \epsilon \quad (17)$$

with both $\bar{\mathbf{a}}_r(\theta)$, the nominal receiving array steering vector, and ϵ being given.

The RCB method is based on the following covariance fitting formulation [5]:

$$\begin{aligned} &\max_{\sigma^2(\theta), \mathbf{a}_r(\theta)} \sigma^2(\theta) \\ &\text{subject to} \quad \hat{\mathbf{R}} - \sigma^2(\theta) \mathbf{a}_r(\theta) \mathbf{a}_r^H(\theta) \geq 0 \\ &\quad \| \mathbf{a}_r(\theta) - \bar{\mathbf{a}}_r(\theta) \|^2 \leq \epsilon, \end{aligned} \quad (18)$$

where $\sigma^2(\theta)$ denotes the power of the signal of interest and $\mathbf{P} \geq 0$ means that \mathbf{P} is Hermitian positive semi-definite. By using the technique in [5], the optimization problem in (18) can be simplified as:

$$\begin{aligned} &\min_{\mathbf{a}_r(\theta)} \mathbf{a}_r^H(\theta) \hat{\mathbf{R}}^{-1} \mathbf{a}_r(\theta) \\ &\text{subject to} \quad \| \mathbf{a}_r(\theta) - \bar{\mathbf{a}}_r(\theta) \|^2 \leq \epsilon. \end{aligned} \quad (19)$$

By using the Lagrange multiplier methodology [5], the solution to (19) is found to be

$$\hat{\mathbf{a}}_r(\theta) = \bar{\mathbf{a}}_r(\theta) - [\mathbf{I} + \lambda(\theta) \hat{\mathbf{R}}]^{-1} \bar{\mathbf{a}}_r(\theta). \quad (20)$$

The Lagrange multiplier $\lambda(\theta) \geq 0$ in (20) is obtained as the solution to the constraint equation

$$\| [\mathbf{I} + \lambda(\theta)\hat{\mathbf{R}}]^{-1} \hat{\mathbf{a}}_r(\theta) \|^2 = \epsilon, \quad (21)$$

which can be solved efficiently by using the Newton method since the left side of (21) is a monotonically decreasing function of $\lambda(\theta)$ (see [5] for more details). Once the Lagrange multiplier $\lambda(\theta)$ is determined, $\hat{\mathbf{a}}_r(\theta)$ is obtained from (20). To eliminate a scaling ambiguity (see [5]), we scale $\hat{\mathbf{a}}_r(\theta)$ such that $\| \hat{\mathbf{a}}_r(\theta) \|^2 = M$. Replacing $\mathbf{a}_r(\theta)$ in (5) by the scaled steering vector $\hat{\mathbf{a}}_r(\theta)$ yields the RCB estimate of $\beta(\theta)$.

5. NUMERICAL EXAMPLES

Consider a MIMO radar system where a uniform linear array with $N = M = 10$ antennas and half-wavelength spacing between adjacent antennas is used both for transmitting and for receiving. The transmitted waveforms \mathbf{s}_n ($n = 1, 2, \dots, N$) are orthogonal quadrature phase shift keyed (QPSK) sequences, and hence we have $\hat{\mathbf{R}}_{SS} = \mathbf{I}$.

Consider a scenario in which $K = 3$ targets are located at $\theta_1 = -40^\circ$, $\theta_2 = -25^\circ$, and $\theta_3 = -10^\circ$ with “reflection coefficients” $\beta_1 = 4$, $\beta_2 = 4$, and $\beta_3 = 1$, respectively. There is a strong jammer at 0° with an unknown waveform and with amplitude 1000, i.e., 60 dB above β_3 . The received signal has $L = 256$ snapshots and is corrupted by a zero-mean spatially colored Gaussian noise with an unknown covariance matrix. The (p, q) th element of the unknown noise covariance matrix is $\frac{1}{\text{SNR}} 0.9^{|p-q|} e^{j\frac{(p-q)\pi}{2}}$.

We first consider the case of no array calibration errors. Let SNR = 10 dB. The moduli of the spatial spectral estimates of $\beta(\theta)$, versus θ , obtained by using LS, Capon and APES are given in Figs. 1(a), (b) and (c), respectively. We show the true spatial spectrum via dashed lines in these figures. As seen in Fig. 1(a), the LS method suffers from high sidelobes and low resolution. Due to the presence of the strong jamming signal, the LS estimator fails to work properly. Capon and APES possess great interference and jamming suppression capabilities. The Capon method gives very narrow peaks around the target locations. However, the Capon amplitude estimates are biased downward. The APES method gives more accurate amplitude estimates around the target locations but its resolution is slightly worse than that of Capon. Note that in Figs. 1(a)-1(c) a false peak occurs at $\theta = 0^\circ$ due to the presence of the strong jammer. Fig. 1 (d) gives the GLR as a function of the target location parameter θ . As expected, we get high GLRs at the target locations and low GLRs at other locations including the jammer location. By comparing the GLR with a threshold, the false peak due to the strong jammer can be readily detected and rejected, and a correct estimate of the number of the targets can be obtained.

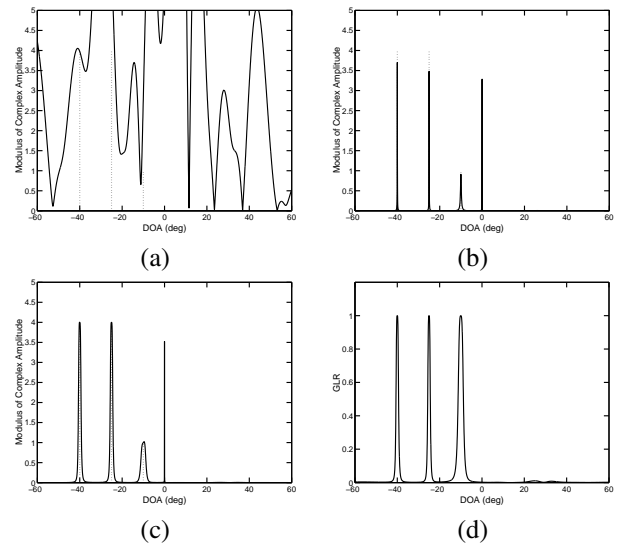


Fig. 1. Spatial spectral estimates and GLR in the absence of array calibration errors. (a) LS, (b) Capon, (c) APES, and (d) GLR.

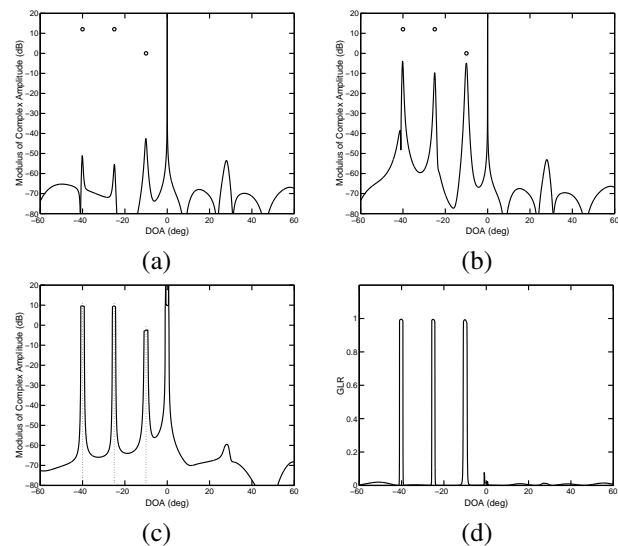


Fig. 2. Spatial spectral estimates and GLR in the presence of array calibration errors. (a) Capon, (b) APES, (c) RCB with $\epsilon = 0.1$, and (d) GLR.

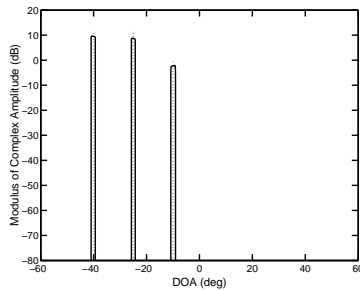


Fig. 3. Refined spatial spectral estimate in the presence of array calibration errors.

We next consider the case where array calibration errors are present. To simulate the array calibration error, each element of the steering vector $\mathbf{a}_t(\theta) = \mathbf{a}_r(\theta)$, for each incident signal, is perturbed with a zero-mean circularly symmetric complex Gaussian random variable with variance 0.005 and then scaled to have norm \sqrt{M} . We let $\text{SNR} = 30$ dB. The other simulation parameters are the same as those in Fig. 1. For the sake of description convenience, the moduli of the amplitude estimates are on a dB scale. As shown in Fig. 2(a), the Capon method fails to work properly in the presence of array calibration errors, as expected: its amplitude estimates at the target locations are severely biased downward (by more than 60 dB for some of them). Although APES gives much better performance than Capon, its amplitude estimates at the target locations are about 10 dB lower than the true amplitudes. On the other hand, RCB provides accurate estimates of the target amplitudes as well as target locations, but their peaks are wider (and hence their resolution is poorer) compared to what is shown in Fig. 1(b), as expected (robustness to array calibration errors inherently reduces the resolution). Again, note that in Figs. 2(a)-2(c) a false peak occurs at $\theta = 0^\circ$ due to the presence of the strong jammer. Fig. 2(d) shows the GLR corresponding to RCB, as a function of θ , which is obtained by replacing $\mathbf{a}_r(\theta)$ in (16) by $\hat{\mathbf{a}}_r(\theta)$ obtained in Section 4. As we can see, high GLRs is given at the target locations and a low GLR at the jammer location. Based on the GLRs, we can again readily and correctly estimate the number of targets to be 3. Plotting the spatial spectral estimates in Fig. 2(c) only for the angles at which the corresponding GLRs are above a given threshold (say 0.8), we obtain the refined spatial spectral estimates in Fig. 3. This refined spatial spectral estimate provide an accurate description of the target scenario.

6. CONCLUSIONS

We have considered several adaptive techniques for a MIMO radar system, where multiple antennas transmit linearly independent waveforms and multiple antennas receive the re-

flected signals. In the absence of array calibration errors, we have considered Capon, APES and GLRT. Capon provides high resolution, APES gives accurate amplitude estimates at the target locations, while GLRT provides good jammer resistant ability. In the presence of array calibration errors, we have shown that the RCB approach can provide accurate estimates of both target locations and target amplitudes.

7. REFERENCES

- [1] E. Fishler, A. Haimovich, R. Blum, L. Cimini, D. Chizhik, and R. Valenzuela, "Spatial diversity in radars - models and detection performance," *IEEE Transactions on Signal Processing*, to appear.
- [2] D. R. Fuhrmann and G. S. Antonio, "Transmit beamforming for MIMO radar systems using partial signal correlation," *Proceedings of the 38th Asilomar Conference on Signals, Systems and Computers*, vol. 1, pp. 295-299, Nov. 2004.
- [3] F. C. Robey, S. Coutts, D. D. Weikle, J. C. McHarg, and K. Cuomo, "MIMO radar theory and experimental results," *Proceedings of the 38th Asilomar Conference on Signals, Systems and Computers*, vol. 1, pp. 300-304, Nov. 2004.
- [4] J. Li and P. Stoica, "An adaptive filtering approach to spectral estimation and SAR imaging," *IEEE Transactions on Signal Processing*, vol. 44, pp. 1469-1484, June 1996.
- [5] J. Li, P. Stoica, and Z. Wang, "On robust Capon beamforming and diagonal loading," *IEEE Transactions on Signal Processing*, vol. 46, pp. 1954-1966, July 2003.
- [6] P. Stoica, Z. Wang, and J. Li, "Robust Capon beamforming," *IEEE Signal Processing Letters*, vol. 10, pp. 172-175, 2003.
- [7] P. Stoica, H. Li, and J. Li, "A new derivation of the APES filter," *IEEE Signal Processing Letters*, vol. 6, pp. 205-206, August 1999.
- [8] E. J. Kelly, "An adaptive detection algorithm," *IEEE Transactions on Aerospace and Electronics Systems*, vol. 22, pp. 115-127, March 1986.
- [9] A. Dogandžić and A. Nehorai, "Generalized multivariate analysis of variance," *IEEE Signal Processing Magazine*, pp. 39-54, September 2003.